# Can structure data obtained from CT images substitute for parameters of a preferential flow model?

A.-S. Lissy, S. Sammartino, S. Ruy

# Can structure data obtained from CT images substitute for parameters of a preferential flow model?

Authors: Lissy A.-S.[(1)(2)], Sammartino S. [*(1)(2)], Ruy S. [(2)]

[(1)] Avignon Université, UMR EMMAH "Environnement Méditerranéen et Modélisation des Agro-Hydrosystèmes", F-84914 Avignon Cedex 09, France.
[(2)] INRAE, UMR EMMAH "Environnement Méditerranéen et Modélisation des Agro-Hydrosystèmes", F-84914 Avignon Cedex 09, France.

* Corresponding author: stephane.sammartino@univ-avignon.fr

Keywords: water flow modeling, Kinematic Wave Dispersion (KDW) model, Richards equation, 3D images, X-ray tomography, sensitivity analysis.

**Highlights:**

- Classical and advanced versions of a water flow dual-porosity model are presented
- Structure parameters from X-ray images are integrated in the advanced version
- Classical version gives best results but water exchange is not properly simulated
- Advanced version produces worse results but a new knowledge has been introduced
- Drainage dynamics (initial state: dried at a matric potential of -3.5 m) is controlled by water exchange among porosity domains

**Abstract**

Modeling preferential flow in soils is still a challenge for the scientific community working on water resources. Indeed, it is an issue to determine the functional parameters of models dedicated to water flow, that are currently obtained by fitting processes, whereas their relationships with soil structure remain poorly known. Improved models are expected from a better understanding of the links between functional and structural parameters, which can be achieved thanks to recent developments in imaging methods such as X-ray Computed Tomography (CT). The paper seeks to improve a dual-porosity model, coupling matrix flow (by Richards equation) and preferential flow (by a Kinematic Dispersive Wave), by substituting some model parameters, usually obtained by inversion of experimental data, by those assessed from CT images of the soil structure. Thus, two versions of the model are compared, the "classical" and the "advanced" one including parameters determined using the 3D images of the sample structures. To compare model versions with real situations, infiltration experiments were conducted in lab on two different soils at two initial water contents. An X-ray medical scanner allowing acquisitions of large soil volumes (≈ 1700 $cm^3$) with a voxel size of 400 µm was used to image the sample structures. Then, we derived two geometrical parameters from the macroporosity network: the percolating macroporosity and a characteristic dimension of this macropore network, the mean inter-macropore distance. The sensitivity analysis conducted on the classical version of the model showed that the kinematic coefficient and the dimensional parameter of the porous medium are the two main contributors to the cumulated drainage whatever the initial condition. Although experimental data are better simulated by the classical version of the model, drainage dynamics is also well simulated by the advanced version. However, differences between the model versions that are small for both soils at field capacity become significant for the dried state (mean initial matric potential of -3.5 m). This emphasizes the crucial effect of the sink-source term and in particular the complex effect of the dimensional parameter that it contains. Indeed, difficulties to simulate properly water exchange between porosity domains are encountered for both versions of the model. We conclude that empirical parameters that were up to now fitted from experiments could be deduced from geometrical indicators computed from CT images and that owning to these first results the applied methodology is promising to achieve a better understanding and modeling of preferential flow processes and to improve model predictability.

## 1. Introduction

Preferential flow in soil concerns all the phenomena by which water and solutes move along certain pathways, while bypassing a large fraction of the porous matrix (Hendrickx and Flury, 2001). Three preferential flow phenomena can be distinguished: finger flow, funnel flow and flow in macropores. While finger flow results from hydrodynamic instabilities at the infiltration front, when crossing soil discontinuities at a mesoscale, macropore flow is associated with porosity heterogeneity at a larger scale such as large interconnected pores (i.e. macropores) distributed within the soil matrix (Germann et al., 2007). Funnel flow can be induced by must larger macroscale heterogeneities (Nimmo, 2012 ; Jarvis et al., 2016)). Macropore flow occurs in a reduced part of the soil macroporosity , i.e. the accessible, more open, and interconnected fraction. This fraction is also called active, functional, percolating or connected macroporosity. Efforts to characterize and dynamically identify this fraction of the pore space have recently been reported (Jarvis et al., 2016; Katuwal et al., 2015; Mossadeghi-Björklund et al., 2016; Sammartino et al., 2015), most of them using the possibilities such as those offered by X-ray tomography to non-destructively image and characterize the internal soil structure. Although relatively little is known about the hydrodynamic processes and associated physicochemical mechanisms at the macropore surface, the effects of macropore flow in soils have been widely studied (Beven and Germann, 2013, 1982). Macropore flow can affect the partitioning between runoff and drainage, the response of the water table to rainfall events, and the groundwater quality as the filtering capability of the soil is not activated for macropore flow (Clothier et al., 2008). To account for preferential flow at soil profile scale, several water-flow models have been developed in the past three decades (Gerke, 2006).

The first models focused on preferential flow processes without accounting for matrix flow. In the macroporous domain, the gravitational movement of water is described by a Kinematic Wave equation (Beven and Germann, 1982; Gerke, 2006). Chen and Wagenet (1992) and Germann (1990) derived a functional relation between the mean water flux and the water content, with a Newton's law on shear and with a channel flow approach and combined this relation with the continuity equation. Thus, they developed the kinematic wave model (KW) for the modeling of fast water flow in macropores (Germann, 1985). Numerous results showed that the KW model was able to accurately simulate infiltration-drainage experiments when preferential flow process is dominant (Di Pietro and Lafolie, 1991; Germann and Di Pietro, 1996). However, results presented by (Germann et al., 1997) showed that the KW model overestimates macropore flow because friction and gravity forces are not balanced immediately in transient flow regime and enhance dispersion of the wetting and draining front. Dispersion of water flow can be induced by the sum of capillary forces, spatial convective inertia effects and resistance forces due to complex pore paths (Di Pietro, 1998). Thus later, (Di Pietro et al., 2003) developed the Kinematic Dispersive Wave (KDW) model as a correction of the KW equation, to take into account fluid dispersion effects due to the local inertia forces that are dominant in large macropores. In the KDW model, it is assumed that the water flux is a nonlinear function of the mobile water content and of its first time derivative. In (Di Pietro et al., 2003), the KDW model was validated by comparison to experimental data. However, it was not coupled to a model, such as the commonly used Darcy-Richards equation for the modeling of slow water flow in the matrix, as is required in complex soils where slow matrix flow and rapid macropore flow can occur simultaneously and promote water exchange between the porosity domains.

Then models based on a dual porosity approach were developed, where each porosity domain has its own hydraulic properties and solute concentrations (Gerke and van Genuchten, 1993; Gwo et al., 1995; Jarvis and Boesten, 1998). These models account for macropore and matric flows, water and mass exchanges between the two domains. The main difference among existing dual-porosity models consists in the approach used to represent macropore flow as the exchange terms are conceptually quite similar, i.e. kinematic waves (Jarvis, 1994), or the Darcy-Richards equation with a high hydraulic conductivity (Gerke and van Genuchten, 1993). Most dual-porosity models have an exchange term between porosity domains which integrates some structural parameters. As far as we know, these parameters account for a mean macropore shape and the spatial arrangement of macropores. However they are not experimentally determined in an independent way, but are usually mathematically calculated with an inversion procedure applied to calibration data (Gerke, 2012). Consequently, most of the time, these parameters serve to adjust the model and their relationships with the structural properties of samples are far from being correctly understood.

The modeling approach that was used in the paper is a model developed by coupling two older models, the KDW model for macropore flow and the Darcy-Richards equation for matric flow. The coupling and modeling works were done using the interactive French modeling platform named Virtual Soil (https://www6.inra.fr/vsoil). The paper is dedicated to the comparison of two versions of this model: one named "classical" in which all parameters are inverted from calibration data, and one named "advanced" in which two parameters selected among the previous ones are independently assessed from the CT images of soil samples. The study was conducted following three steps. Firstly, a sensitivity analysis was realized for a better understanding of the parameter sensitivity of the classical version of the model. Secondly, this version was used to simulate the infiltration-drainage experiments performed on the undisturbed soil columns under simulated rainfalls and for contrasted initial soil moistures (the field capacity and the dried state at -3.5 m of matric potential). Parameters of the classical model version were adjusted on calibration data for each soil and experiment. Thirdly, the additional knowledge provided by the CT images of sample structures was introduced in our model to create the advanced version. Two structure features of the soils were derived: the volume of the percolating =macroporosity and a dimension of this percolant network, which was chosen to characterize the spatial distribution of macropores over the sample height: the mean inter-macropore distance. These parameters were then integrated in the advanced version of the model. The quality of the cumulative drainage and storage simulated during infiltration experiments and the distribution of water flow in the porosity compartments are finally discussed.

## 2. Materials and Methods

### *2.1 Soil sampling and soil characteristics*

Two undisturbed soil cores of two different soils with contrasted textures and structures were sampled for the infiltration experiments (Table 1). The first one is a Loamy soil (Calcisol Chromic Cambisol, WRB) with a grainy structure (43.948790, 4.461378). The second one is a Silty soil (Calcaric Fluvisol, WRB) with polyhedral aggregates due to shrinkage and swelling of clay minerals and showing numerous tubular macropores due to earthworm activities (43.915343, 4.882514).

Two additional samples were collected for each soil to determine the hydric properties of the soil matrix with Wind’s evaporation experimental setup (Wind, 1969). As the Wind sample is 7 cm in height (15 cm in diameter), hydrodynamic properties were determined on two soil layers, each 7 cm in height. This total layer of 14 cm is strictly included in the first soil horizon. The sampling of columns and Wind samples followed the protocol given by (Tamari et al., 1993) to extract soil cores with minimal disruption. A soil column was obtained by slowly inserting a PVC tube (12.5 cm inner diameter and 20 cm height), equipped with a sharp cutting tool at its end, into the soil while step-by-step gently removing the soil around the tube to minimize friction and shear forces. After sampling, a PVC grid with 1 mm diameter holes drilled every 1.5 mm was stuck at the bottom of the column to restrain the loss of soil aggregates during water drainage. The grid is not necessary for Wind samples and their sample holder is a metal ring (7 cm height) drilled every 1 cm in height for the lateral insertion of pressure probes. Columns and Wind samples were stored enclosed in a plastic bag at 4 °C to avoid germination and earthworm displacement before the first experiment. A small quantity of chloroform was poured on the upper surface of the column samples in order to stop soil macrofauna activity and avoid soil structure evolution during storage and experiments.

For each soil, one column was used for infiltration experiments and 3D X-ray image acquisition of soil structures. The second one was equipped with 6 pressure probes for monitoring the evolution of the matric potential in order to determine the distribution of the initial water content over the sample height. The soil columns thus equipped were not scanned but remained in the laboratory. It is important to mention that these twin columns (those for infiltration experiments and those for the recording of matric potential) underwent the same history since their sampling (same storage conditions, same infiltration experiments, same delay between experiments). The sample drying was a slow drying at the controlled ambient conditions of the air-conditioned lab (mean temperature of 22°C and mean air humidity content of 45%). The infiltration experiments and the image acquisitions of soil structures were thus conducted at two initial water contents, 1) the field capacity which means that soil matrix should be saturated and the percolating macroporosity should have drained, and 2) a drier water content intermediate between the field capacity and the wilting point of plants, named “dried at h = -3.5 m”. The state is reached when the mean of the pressure probes of the equipped columns indicate a matric potential near of -3.5 m. In the following text and legends, the moisture status “dried at h = -3.5 m” can be indicated by “DS” as well as the field capacity by “FC”.

*2.2 Soil hydrodynamic properties*

Wind samples are used for the determination of soil hydraulic properties (water retention and hydraulic conductivity curves). Hydraulic conductivity of the saturated soil ($K_{sat\text{-}meas}$, m.s$^{-1}$) was measured using a constant head permeameter (Dirksen, 1998). The $K_{sat\text{-}meas}$ of undisturbed samples was measured including all porosities (micropores and macropores). Soil matrix hydraulic properties were determined with the Wind evaporation method (Tamari et al., 1993; Wind, 1969). Retention and hydraulic conductivity curves were fitted by the Wind algorithm that uses the Mualem-van Genuchten model (Schaap and Leij, 2000; Van Genuchten, 1980). The porosity (ε) was calculated using the relation between bulk density

($\rho_d$) and soil particle density ($\rho_s$): ($\varepsilon = 1 - \frac{\rho_d}{\rho_s}$). All the hydrodynamic properties are summarized in table 2.

*2.3 Device and infiltration experiments*

A specific device that was designed to be placed in a medical scanner was used (Fig.1). It allows the recording of water fluxes together with discrete acquisitions of 3D images during a rainfall event simulated inside the scanner. The device structure is made of wood without any metal parts. The soil core is placed on the wooden table which is supported by two precision scales (B1 and B2) to measure soil column weight during the infiltration-drainage experiment. A third precision scale (B3) measures the water quantity drained at the sample bottom. The three scales are connected to a computer and recorded continuously during the experiment from the beginning of rainfall to the drainage after the rainfall is stopped. No scales or metal parts are included in the field of view of the scanner to avoid scanning artifacts. The rainfall simulator is composed of a plastic tank with hypodermic needles arranged on a squared mesh on the bottom surface (0.4 mm inner diameter every 1.5 mm). It is connected to a pulse pump whose piston volume and pulse frequency are adjusted to control the simulated rainfall intensity.

Three preliminary infiltration experiments were performed in the laboratory to gradually saturate the soil in order to reach the field capacity. This water content is a conceptual vision of the water distribution in which the soil matrix is assumed to be fully saturated with macropores completely drained. During these first experiments, water fluxes and column weight were also measured to control the mean water content. Following these preliminary tests, two rainfalls were made inside the medical scanner, the first one at field capacity and the second one far from the field capacity (dried to a water potential of 3.5 m). For each rainfall event, the rainfall simulator was set to deliver intensity near of 20 $mm.h^{-1}$ for duration of one hour and a half. These values were chosen to simulate a thunderstorm that usually occurs several times per year in the French Mediterranean region. Each simulated rainfall event delivered 30 mm of water to the soil. The weight of the soil column was recorded every 10 s from the beginning of the rainfall to half an hour after stopping the rainfall (120 min.). Throughout the duration of the experiment, several 3D images were acquired to monitor water infiltration within the soil core but for this study we used only the first image acquired before the rainfall event began, taken as the reference for the initial soil structure and water content. At field capacity, the rainfall intensity was 20.2 $mm.h^{-1}$ and the initial mean matric potential was around -0.05 m for the Loamy soil (resp. 20.5 $mm.h^{-1}$ and -0.15 m for the Silty soil). In the initial wet state, the rainfall intensity was 23.5 $mm.h^{-1}$ for the Loamy soil (resp. 21.7 $mm.h^{-1}$ for the Silty soil) and the initial mean matric potential was around -3.5 m for the two soil samples.

*2.4 The flow model accounting for preferential flow*

The model simulates slow water flow driven by capillarity and gravity in the soil matrix with the Richards equation and fast gravity-driven flow in the macroporosity with the Kinematic Dispersive Wave equation (Di Pietro et al., 2003). Water flow between the two soil porosity domains is calculated by a sink-source term.

*2.4.1 Richards equation*

The Richards equation for the soil matrix:

$$\frac{\partial \theta_{mi}(h)}{\partial t} + \frac{\partial}{\partial z}\left(-K_{mi}(h)\frac{\partial (h-z)}{\partial z}\right) = S \; ; \qquad \text{[Eq. 1]}$$

where: $\theta_{mi}$ ($m^3.m^{-3}$) is the water content of the soil matrix; $h$ (m) is the matric potential; $K_{mi}$ ($m.s^{-1}$) is the hydraulic conductivity of the soil matrix, $S$ ($m^3.m^{-3}.s^{-1}$) is the sink-source exchange term and is described in the following section.

*2.4.2 Kinematic Dispersive Wave and sink – source term*

As stated by Di Pietro et al. (2003), when non conservative forces that induce attenuation of the kinematic water wave are present, the macroscopic water flux $q_{ma}$ depends on the mobile water content $\theta_{ma}$ and also on its derivatives. In Di Pietro et al. (2003), a time derivative of $\theta_{ma}$ was chosen to account for these inertial forces. In this paper the time derivative is replaced by a space derivative for improving the numerical resolution and reducing numerical defaults. The $q_{ma}(\theta_{ma})$ relationship is now written as:

$$q_{ma} = b\theta_{ma}^{a} - \nu_\theta \frac{\partial \theta_{ma}}{\partial z} \qquad \text{[Eq. 2a]}$$

where: $b$ ($m.s^{-1}$) is the kinematic coefficient, $a$ (–) is an empirical parameter qualitatively related to the shape of the macropores and the laminar/turbulent nature of water flow in macropores (Ruy et al., 1999). $\nu_\theta$ ($m^2.s^{-1}$) is similar to a diffusion coefficient and account for the importance of inertial effect and capillary diffusion compared to the pure convective effect of the KDW model (Di Pietro et al., 2003). Introducing this relationship in the water balance equation of the macropore network and taking into account the exchange term with the matrix domain leads to the following equation:

$$\frac{\partial\theta_{ma}}{\partial t} + c\,\frac{\partial\theta_{ma}}{\partial z} - \nu_\theta\,\frac{\partial^2\theta_{ma}}{\partial z^2} = -S \qquad \text{[Eq. 2b]}$$

where $\theta_{ma}$ is the water content in macropores; $c = \left.\frac{\partial q_{ma}}{\partial\theta_{ma}}\right]_{\frac{\partial q_{ma}}{\partial z}=cte} = ab\theta_{ma}^{a-1}$ (m $s^{-1}$) is the velocity of the infiltration front.

The Richards and the KDW equations are coupled with the exchange term *S* (Eq. 3) which is slightly modified from (Ruy et al., 1999) by assuming that the water potential in the macropore network is equal to 0:

$$S = -\frac{K_{mi}(h)}{d} \times \frac{-h}{d} \times \frac{\theta_{ma}}{\theta_{max-mac}}; \qquad \text{[Eq. 3]}$$

where: $d$ (m) is a shape parameter of the macroporosity, a characteristic size of the porous media, called inter–macropore distance in the rest of this article; $\theta_{max-mac}$ ($m^3.m^{-3}$) is the saturated water content in the macroporosity.

*2.4.3 Estimation of KDW and sink – source term parameters*

Two versions of the model were studied and compared. The first version, named “classical”, corresponds to the modeling where the unknown parameters of the model are fitted from rainfall-drainage experiments by an inverse modeling method. The second version, named “advanced”, corresponds to an innovative modeling where the unknown structural parameters used in the sink term are computed from an advanced processing of 3D images of the soil structure.

- ***Classical version of the model***

KDW ($a, b, \nu_\theta$) and sink – source term ($d$ and $\theta_{max-mac}$) parameters were estimated using the DREAM algorithm for each of the four experiments. This method is a global optimization algorithm that provides an exact Bayesian estimate of uncertainty (for more details see (Vrugt, 2016; Vrugt et al., 2008).

The variation range of each parameter is presented in Table 3. However, as *a* and *b* are correlated (Ruy et al., 1999), we could not use the DREAM algorithm directly. To deal with this correlation, we assumed that the hydraulic conductivity of the measured saturated soil matrix can be neglected compared to the water flow in the macropore network. This assumption is based on the measured value of $K_{sat-meas}$ obtained on undisturbed soil cores with large macropores that is more than two orders of magnitude higher than the calculated value of $K_{mi}$ obtained with the Wind's method at matrix near saturation. Thus, we obtain the following relationship for the flow at steady state under a unit gradient and full saturation of the soil core:

$$K_{sat-meas} \approx b \cdot \theta^{a}_{max-mac} \qquad \text{[Eq. 4]}$$

where $K_{sat\text{-}meas}$ is the hydraulic conductivity measured previously in the laboratory, and $b \cdot \theta^{-a}_{max-mac}$ is the water flux through the macroporosity. Eq. 4 shows that for a given soil, parameters $b$ and $a$ are not independent. In the first step, the value of $a$ was successively set to $1, 2, 3, 4, 5, 6$. For each value of $a$, a theoretical value of $b$ was computed from Eq. 4 by using the median value of measured macroporosity profile $\theta_{\max-mac-meas}$:

$$b_{th} = K_{sat-meas} \times \theta^{-a}_{max-mac-meas} \qquad \text{[Eq. 5]}$$

This value was used to set the variation range in which the DREAM algorithm searches the value of $b$ for fitting, see Table 3. For each value of $a$, DREAM fits the set of parameters ($b$, $d$, $v_\theta$ and $\theta_{max-mac}$) by minimizing the error between observation and simulation curves. We then defined a restricted search interval for $a$ according to the lower temporal error. This restricted interval is used in the second step whose purpose is the estimation of all parameters ($a$, $b$, $d$, $v_\theta$ and $\theta_{max-mac}$) using the DREAM algorithm on restricted intervals for $a$ (search intervals [$a_{min}$ ; $a_{max}$]) and $b$ search interval as :

$$\left[\frac{(K_{sat-meas} \times \theta^{-a_{max}}_{max-mac-meas})}{5}; (K_{sat-meas} \times \theta^{-a_{min}}_{max-mac-meas}) \times 5\right] \qquad \text{[Eq. 6]}$$

Search intervals for other parameters are reported in Table 3. Experiments were simulated with these parameter sets, and the final fitting was evaluated using the temporal error curve.

- ***<u>Advanced version of the model incorporating additional knowledge provided by the 3D imaging.</u>***

The assumption behind the advanced version of the model was that some parameters, which are usually estimated by inversion, could be replaced with the data obtained independently thanks to the 3D images of the sample structure. In this advanced version, KDW parameters ($a, b$ and $v_\theta$) are estimated by the DREAM method as was the case in the classical version, but two parameters ($d$ and $\theta_{max-mac}$) controlling the sink-source are obtained thanks to image data. Moreover, we replace a unique value of two sink-source term parameters by a profile of around 400 values measured over the height of the soil column which permits accounting for soil structural heterogeneity and the unidirectional nature of the model on the Z-axis. The fitting methodology of KDW parameters is the same as previously.

*2.4.4 Sensitivity analysis*

The sensitivity analysis was performed to increase our model understanding in the transient and pseudo-stationary regimes and to quantify the importance of each parameter and their interaction effects. The study was conducted in particular to highlight the effect of initial water content on parameter sensitivity using the classical version of the model.

The sensitivity analysis (SA) was performed on one model output recorded during experiments: the cumulative water drainage. The SA was conducted on parameters of the KDW model and of the sink-source exchange term using the FAST 99 method based on the Fourier Amplitude Sensitivity Test. This method estimates the contribution of each input factor to the output's variance (Saltelli et al., 1999); the chosen variation ranges are the same as those for the first step of the DREAM estimation (Table 3). FAST calculates two indexes for each parameter: (1) the principal contribution, and (2) the total contribution, to the variance of the output variable. For a given parameter, the difference between the two indexes represents the interaction effects of this parameter with the other parameters: it is the part of the output variable variance explainable by interactions between all tested parameters.

*2.5 X-ray scanner, acquisition and image processing methods*

Helical acquisition is designed to strongly diminish the acquisition time of medical scanners. This device was therefore chosen to acquire the reference image taken before the rainfall was started and the series of time-resolved images that were not used in this study. The images were acquired with a Siemens SOMATOM Definition AS 128 slices CT scanner, equipped with multi-detector rows that can acquire 128 slices simultaneously. It is located in the "Val de Loire" center of the French National Institute for Agricultural Research and Environment (INRAE); for more details see (Sammartino et al., 2015). The system setting to optimize acquisition is an acceleration voltage of 140 kV, a tube current of 400 mA, and a pitch factor of 0.35. The table feed is 12.35 mm.s$^{-1}$. The entire soil volume is thus scanned in 10 s.

*2.5.1. Pre-processing and macroporosity thresholding*

Tomographic sections were reconstructed using the Siemens software that applies a filter to enhance object edges and remove beam hardening. No more additional information can be obtained on the reconstruction step. In medical tomography, the image grey levels are calibrated to the Hounsfield scale which transforms attenuation coefficients into local bulk densities, based on the X-ray attenuation by water and air. Tomographic images are given in the 12-bit signed DICOM format (Raw CT data). Pre-processing and processing of image series were applied by following the methodology given in Sammartino et al. (2012). At the end, the sample holder is removed from the region of interest, images are cropped and resliced in order to obtain cubic voxels with a side of 400 µm, and a forbidden color is applied to the background. The macroporosity thresholding was also performed according to the procedure given in Sammartino et al. (2012) that uses a mixing law between air, infiltration water and soil matrix, and hypotheses on the voxel content to determine the thresholds to apply. Indeed, as these images are calibrated in "density" by the Hounsfield scale, a simplified attenuation model was developed and used. It is based on X-ray attenuation of water and soil matrix, and on the porosity and water saturation. Making hypothesis on the distribution of water, air and soil matrix in one voxel, values of the thresholds in the Hounsfield scale can be calculated using the simplified model (Sammartino et al. 2015). Owing to the voxel size, all the voxels fulfilled with air or water were classified in the macroporosity compartment. By following this approach having in mind an image analysis point of view, all the voxels fulfilled with more than half air or water were also classified in macroporosity. The other voxels were put in the soil matrix compartment. The applied thresholds in the Hounsfield scale were respectively for the field capacity and the dried state at -3.5 m, 468 and 478 for the loamy soil, and 498 and 510 for the Silty soil. After thresholding, the quality of segmentation was checked on several slices randomly chosen in the stacks by superimposing outlines of the macroporosity phase on grey level images in a transparent-paste mode. Then, the raw CT data were transformed into binary images from which morphological and topological parameters associated with the macropore networks can be quantified. All the pre-processing was performed with ad-hoc macros and plugins developed and used with the public domain software ImageJ (Schneider et al., 2012).

### *2.5.2. Determination of new parameters for the dual-porosity model*

We focused on the percolating =macroporosity as described by Sammartino et al. (2015), i.e. the interconnected pathways within which fast flow can occur under gravity. These authors showed by adding brilliant-blue to a water infiltration experiment that the active part of the porosity was quite similar to the percolating part of the macroporosity, i.e. the macropore network that connects the input and output surfaces of the soil column. To derive this percolating network from the whole macroporosity, the tool “Axis connectivity” of Avizo® was applied in the column height direction. This tool is usually used to segment the part of porosity that is connected to the input and output surfaces of a sample in a given direction. In three-dimension, the structuring element was a 26-voxels neighborhood and the propagation axis, the Z-axis (sample height). Macropores are labellized and then we retain the most important one that connects both sample sections.

The sink-source term defined previously, which controls lateral flow from macropores to the soil matrix, depends on a characteristic size of the porous medium. This dimension is usually assimilated to a representative aggregate size by analogy to homogeneous porous media. In heterogeneous porous media, such as macroporous soils, it seemed necessary to account for the spatial distribution of structural heterogeneities in the definition of this characteristic size. We chose to determine the average half-distance between macropores of the percolating macroporosity using a Voronoï Diagram (named after the mean inter-macropore distance). This diagram gives a set of points that have an equal distance to the closest objects, i.e. the medial axis between objects. The average half-distance is obtained at each slice and objects are thus considered as macropore sections intercepted by each slice (Fig. 2e). The inter-macropore distance profile is calculated with an ad-hoc R script (Fig. 2g). Fig. 2 sums up the main processing steps applied to the 3D images. At the end, inter-macropore distances and percolating macroporosity profiles are obtained and discretized on approximately 400 values on sample height.

## 3. Results

### *3.1 Classical version of the model*

#### *3.1.1 Sensitivity analysis (SA)*

Fig. 3 presents the temporal evolution of the principal index (dotted lines) and total contribution index (solid line) for each tested parameter of the KDW model and of the sink-source term. The SA was performed for the two studied soils at two initial moisture conditions for different values of *a* ranging from 1 to 6. However only one value of *a* per graph is presented as results obtained for other values do not significantly change the hierarchy of indexes and the conclusions drawn. The grey shaded area on each graph shows the variability of the cumulative drainages calculated over the 1200 runs of the SA. When the area reaches the x-axis, as shown in Fig. 3b and 3d, this means that breakthrough did not occur in at least one of the runs. Before the start of drainage (roughly between 500 and 1000 s), parameters *b* and $\nu_\theta$ of the KDW model and parameter *d* of the sink-source term are the main contributors irrespective the soil and the initial soil moisture condition. The impacts of these parameters on the cumulative drainage are mainly due to parameter interactions as the principal contribution index is far below the total contribution index.

The contribution of a given parameter to variations in cumulative drainage is a function of time after the drainage onset and this evolution may depend on the soil, on the initial soil moisture and also on the parameter itself. However, the impact of parameter $\nu_\theta$ depends neither on the soil type nor on the initial soil condition: it always decreases with time and its principal order index is about 0. Therefore, this parameter has no or only very little direct impact on the overall cumulative drainage.

At field capacity initial condition, Loamy and Silty soils behave differently. Cumulative drainage of Loamy soil is mainly sensitive to parameter $b$ and then to parameter $\theta_{max-mac}$, and the influence of the parameter $\theta_{max-mac}$ increases with time. Cumulative drainage of Silty soil is sensitive to $b$, $d$ and $\theta_{max-mac}$ parameters. However, for Silty soil at the end of the simulation ($t = 7200\ s$), the principal contribution index of parameter *d* is about 0.5. This means that about 50 % of the variation of cumulative drainage at $t = 7200\ s$ is due to variations in the value of parameter $d$. For this soil, that has not been rehydrated enough by the three preliminary rains, the field capacity initial condition did not exactly correspond to the saturation of the soil matrix (matric potential around -0.15 m).

In the initial dried state (h = -3.5 m), the cumulative drainage is mainly sensitive to parameter $d$ of the sink-source term and then to parameters $b$ and $\theta_{max-mac}$, d and $\theta_{max-mac}$ have an impact on the quantity of water entering the soil matrix from the matrix-macropores interface. The greater $d$ is, the lower the quantity of water entering the soil matrix is and the greater the cumulative drainage is.

### *3.1.2 Parameter adjustment by DREAM inversion*

The cumulated drainage was used to adjust model parameters with the DREAM algorithm and water stored was taken as validation-verification data.

#### 3.1.2.1 Calibration

Simulated and observed cumulated drainage curves are presented in Fig. 4 as well as the time evolution of error between observed and simulated curves. Data from the advanced version of the model will be discussed in part 3.2.

The graphs on the top line show a very close agreement between simulated and measured cumulative drainages. At the end of the experiment, the difference between the total amount of the simulated and measured drainage was less 1 mm (about 3 to 4% of the total amount of measured drainage). The central part of the graph, which represents the quasi-steady state of the infiltration-drainage experiment, is very well simulated. According to the temporal error evolution, estimations are noticeably better for experiments initially at field capacity than for those initially at the state dried at h = -3.5 m. In detail, the first transition between flow regimes can be highlighted by an increase in the error curve. Indeed, error values are always small before breakthrough and increase during breakthrough, characterizing a less accurate estimate of drainage during this transient state.

The main differences can be observed at the beginning of the experiment (drainage onset and breakthrough time) and small differences can be observed at the end of the experiment (end of pure drainage after the rainfall was stopped).

#### 3.1.2.2 Verification on water storage

The total amount of water stored in the column during the infiltration experiment was used to verify the model prediction after parameter calibration. As shown in Fig. 5 (top line), (i) before water breakthrough, the amount of stored water increases linearly with the water supplied by the rainfall simulator, (ii) after this transient state, a quasi-stationary flow regime is reached. The slope of the plateau indicates whether water exchanges occur between macropores and the soil matrix (non-zero slope) or not (zero slope).

The main discrepancies between simulations and measurements occur during the transient state at the drainage onset: the amount of water stored in the soil column may be greatly overestimated (resp. underestimated) for the Loamy soil (resp. Silty soil) in the field capacity initial condition (resp. in the initial dried state at -3.5 m). However at the end of the experiments, differences between the simulated and measured amount of water stored in the soil column are small: they are always less than 1 mm (resp. 2 mm) for a measured water amount of 3 mm (resp. between 6 to 11 mm) in the field capacity initial condition (resp. in the initial dried state at -3.5 m). Moreover, it can be seen that the simulated curve is parallel to the measured curve in the central part of each graph, whatever the initial soil water content. The central part of each graph corresponds to the pseudo steady-state. This part can be almost flat when the quantity of water entering the soil matrix from the macropore walls is negligible, which is the case in the field capacity initial condition. The slope of this part can be positive when water flow from macropores to the soil matrix is significant, which is the case for the initial dried state at -3.5 m Considering that simulated and measured curves are parallel, this means that water flow from macropores to the soil matrix is well simulated by the model. Finally, at the end of the experiments, the discrepancy between simulated and experimental data ranges between 0 and 0.5 mm for simulations conducted in the field capacity initial condition and between 0.7 and 1.1 mm for simulations conducted in an initial dried state. All the parameters estimated are given in table 4.

### *3.2 Advanced version of the model*

The sensitivity analysis showed that the characteristic dimension of the porous media (*d*) and the saturated water content in the macroporosity, i.e. the maximum accessible volume of macroporosity ($\theta_{max-mac}$) are two highly sensitive parameters of the model. We assumed that these parameters could be measured thanks to the 3D images of our undisturbed soil columns obtained from the X-ray scanner. They were thus assessed respectively by the inter–macropore distance and the percolating macroporosity.

#### *3.2.1 CT image*

##### 3.2.1.1. Global properties

The mean inter-macropore distance, the percolating and entire macroporosities are presented in table 5 for both initial water contents. The 3D renderings of the macroporosities in figure 6 underscore the high complexity of the porous structures studied and consequently the challenge of giving a synthetic understandable representation. As a first understanding, samples seem to have macroporosities with variable extents and shapes. Some tubular macropores can be identified and associated to earthworm activity, whereas numerous isolated macropores can be associated with the aggregated structure. The percolating macroporosity is more extended in the Silty soil than in the Loamy one.

The average properties of entire and percolating macroporosities given in table 5 show that these macroporous structures are well above the percolation threshold, with 70 to 85 % of the macroporosity connected and percolating, respectively for Loamy and Silty soil.

At field capacity, the macroporosity of the Loamy soil is 23 % greater than that of the Silty soil, whereas it is almost equal when the initial matric potential is dropped to -3.5 m. For the Loamy soil (respect. Silty soil) containing 14% of clays (respect. 45% of swelling clays), the macroporosity increases of 3% (respect. 27%) from field capacity to the dried state at h = -3.5 m. The macroporosity variations from the field capacity to the dried state at h = -3.5 m, and between soils, depends on clay content and mainly result of an internal shrinkage of the soil matrix with negligible variations of the global sample height.

The behaviour of the percolating macroporosity is identical to those of entire macroporosity and whatever the soil when the initial moisture condition is changing from the field capacity to the wet state: the macroporosity increases and the mean inter-macropore distance decreases. However, this induces small variations for Loamy soil and more significant

variations for the Silty sample (Table 5). Indeed, macroporosity of the silty soil changes from 7.2 to 9.3 % (variation of 27 %) and those of the loamy soil, changes from 7.7 to 8.2 % (variation of 6 %). A same tendency can be seen for the mean inter-macropore distance.
The macroporosity of the Loamy sample, which is more diffuse (Fig.6), shows the smallest mean inter–macropore distance, slightly dependent on the initial moisture condition , in the order of 4 to 5 mm. This distance is multiplied by two when accounting for the percolating macroporosity. For the Silty sample, this increase is much smaller but more dependent on the initial moisture condition, as shown by the 7.8 mm value of the percolating macroporosity in the initial dried state at h = -3.5 m.

#### 3.2.1.2 Profiles of macroporosity and inter-macropore distance properties

Visualizing and analyzing macroporosity variations on sample height is important because of the mono dimensional nature of the model oriented on the vertical axis, Z (Fig. 7). Z-profiles of Loamy soil macroporosity provide the crucial information that the overall shape of the profile does not evolve according to water content or when comparing entire and percolating macroporosity. These profiles are almost superimposable by translation. Their vertical shifts reflect the overall evolutions given in Table 5. The most significant deviations, although weak, are present in the lower part of the column between 0.10 and 0.14 m depth, for the profile of the percolating macroporosity in the case far from the field capacity (column a, light blue dotted line in Figure 7). The same remarks can be made for Silty soil on the shape profiles similarity, with however increasing discrepancies when moving from 0.05 m depth towards the column top. This is probably due to a preferential drying from the column top.

### *3.2.2 DREAM inversion*

Results of the calibration and the validation steps for the advanced model version are presented respectively by green curves in Figures 4 and 5.

#### 3.2.2.1 Calibration

Water drainage simulated by the advanced version of the model is close to the observed data and to simulations obtained with the classical version for soil cores at field capacity (Fig. 4). For the initial dried state at h = -3.5 m, small differences between simulation and measurements can be observed for the Silty soil: the simulated breakthrough time is considerably lower than the observed one and the slope of the simulated curve in the central part of the graph is lower than the experimental one. The result is a slight underestimation of about 4 % of the overall water amount drained out of the soil core. These differences between simulation and measurement are larger for the Loamy soil in the initial dried state and the model underestimates the drained water amount by 18 %. These results are both due to an overestimation of the rewetting of the soil matrix by the advanced model version.

#### 3.2.2.2 Validation – Verification

The water storage simulated by the advanced version of the model is close to observations and simulations made by the classical version for samples initially at field capacity. The gaps between simulated and measured data are also similar (Fig. 5). For the Silty soil at the initial dried state at -3.5 m, the global dynamic is close to the observation for the both models' versions but the rewetting phase of the soil matrix occurring between 500 to 5400 s is more poorly simulated by the advanced version of the model than by the classical one. For the Loamy soil in the initial dried state, the advanced version of the model fails to reproduce the water flow dynamic, contrary to the classical one.

## 4. Discussion

### *4.1 Sensitivity of model parameters*

Sensitivity analysis (see Fig 3) applied to the classical version of the model showed that the kinematic coefficient (*b*), the inter–macropore distance (*d*) and to a lesser extent the maximum accessible macroporous volume ($\theta_{max-mac}$) are the main controlling parameters of the model outputs (drainage and water storage). By applying the sensitivity analysis in two realistic initial moisture conditions, we also outline that the model is sensitive to the initial water content.

At field capacity the kinematic coefficient (*b*) is the most sensitive parameter whereas the inter-macropores distance (*d*) is a sensitive parameter for Silty soil only. As there are no or few water exchanges between the two porosity domains, the model is less sensitive to the parameters involved in the sink–source term, such as $d$ *or* $\theta_{max-mac}$. Moreover, the sensitivity analysis shows a high index of interaction between $b$ and $\theta_{max-mac}$ parameters for Loamy soil and between $b$, $\theta_{max-mac}$ and $d$ parameters for Silty soil: compensation effects between those parameters are likely to occur during the second part of the infiltration experiment.

The high sensitivity to parameter *b* was also underlined by Di Pietro et al. (2003) for the KDW model. Parameter *b* is related to the flow velocity in the macropore network: the model is very sensitive to this parameter when macropore flow is the dominant process of water flow and when rewetting of the soil matrix from macropore walls is negligible, which is the case for the field capacity initial condition. For Silty soil, we suppose that the field capacity initial condition was not fully achieved so that a residual rewetting of the soil matrix was still possible during the infiltration experiment.

At the dried state (h = -3.5 m), $b$ and $d$ parameters are the two sensitive parameters. The compensation index is less important, so there is probably less interaction effect between those parameters for the dried state than at field capacity. The breakthrough time constitutes a limit between the dominance of the kinematic coefficient contribution (before breakthrough) and the dominance of the inter–macropore distance ($d$) that increases and becomes important after breakthrough.

The $\nu_\theta$ parameter that controls kinematic wave attenuation has only a negligible influence on the variance of cumulative drainage over time whatever the initial hydric situations, as already noticed by Di Pietro et al. (2003). However, this parameter linked to the dispersive process of the water flow is essential to reproduce the smooth transitions between the different flow phases: beginning of the drainage after breakthrough, transition to the pseudo-steady-state and beginning of the drainage recession after rainfall has stopped.

To conclude, as a rule of thumb, we can say that:

- (i) the parameter $\nu_\theta$ of the KDW model has practically no or only very little impact on the cumulative drainage, whatever the soil and the initial soil moisture condition;
- (ii) the parameter $b$ of the KDW model is the main sensitive parameter of the cumulative drainage for the field capacity initial condition;
- (iii) the parameter $d$ is the most sensitive parameter to the cumulative drainage for the initial dried state,
- (iv) parameters $b$, $d$ and $\theta_{max-mac}$ show significant interactions, mainly at field capacity initial condition It is important to find a way to independently measure parameter $d$ and $\theta_{max-mac}$ to avoid interactions and possible compensation effects with parameter $b$.

### *4.2 Parameters of the sink-source term*

In Table 4, fitted $d$ and $\theta_{max-mac}$ parameters can be compared to the same parameters obtained for X-ray CT images. Fitted value of $\theta_{max-mac}$ may be slightly different to the mean value of the $\theta_{max-mac}(z)$ profile calculated from CT images: the difference may range between 2% (Silty soil at h = -3.5 m) to 30% (Silty soil at field capacity). On the one hand,

$\theta_{max-mac}$ parameter is not a very sensitive parameter of classical model (see Fig. 3) and its sensitivity is due to interaction effects with others parameters ($d$ and $b$) therefore the fitted value of $\theta_{max-mac}$ may be estimated with a large uncertainty. On the other hand, this parameter has a nonlinear impact on the overall water flow dynamic as the sink source term is inversely proportional to $\theta_{max-mac}$ (see eq. 3): the $\theta_{max-mac}(z)$ profile may therefore not be directly replaced by a single value.

We also observe that the fitted value of $d$ is 3 et 10 times higher than the mean value of *d(z)* profile calculated from CT images. Three hypotheses are proposed to explain this discrepancy. Firstly, as for $\theta_{max-mac}$ parameter, $d$ parameter has a nonlinear impact on the overall water flow dynamic as the sink source term is inversely proportional to the square of $d$ (see eq. 3): the *d(z)* profile may therefore not be directly replaced by a single value. Secondly, different values of $d$ parameter can be compensated by different values fitted for other parameters when the model is sensitive to those parameters. This is particularly the case for parameter $b$ that is a very sensitive parameter whose fitted values may range over several order of magnitude as already observed by Di Pietro et al. (2003) for the KDW model and Di Pietro and Lafolie (1991) for the KW model. Thirdly, the $d$ parameter obtained from CT images may not be directly used in the sink-source term (eq. 3). Indeed, the unique numerical parameter $d$ in eq. 3 stands for two physical parameters: a characteristic length of the mean size of aggregates (or mean distance between macropores) and a characteristic length of water diffusion from macropore walls within the inter-aggregate's spaces inside soil matrix. Eq. (3) is quite similar to sink – source terms found in MACRO (Jarvis et al., 1991) or in Gerke and van Genuchten (1993). The characteristic inter-macropore distance can be extracted from 3D CT image analysis, but the typical water diffusion length cannot be deduced from these images and should be less than the characteristic inter-macropore distance. Therefore, Gerke and van Genuchten (1993) or MACRO (Jarvis et al., 1991) introduced an empirical correcting factor in the sink-source term expression, which was not used here.

### *4.3 Dynamic of water exchange from macropores to soil matrix*

The instantaneous profiles of water exchange rate from macropores to the soil matrix are computed and are given on Fig. 8 for the advanced model version (similar results can be found for the classical one) at10 specific times ranging from the beginning of infiltration before the breakthrough, during the pseudo-steady-state flow and up to the final phase. At the beginning of the experiment, water exchanges occur in the topsoil. Then a "water exchange front" appears and propagates downwards over time . At the end of the rainfall event (t = 5400 s), the water exchange front is located in the deepest part of the soil column and it vanishes as water drains out of the macropores.

For a given soil, the overall exchange rate and its evolution over time is a function of the initial soil condition. For the Loamy soil at field capacity, the exchange rate is always less than $1.10^{-5}$ $m^3.m^{-3}.s^{-1}$ and is mainly located in the upper part of the soil column: at field capacity, its water retention capacity is close to zero and the horizontal gradient of the soil matric potential which is the driving force of water flow from macropores to soil matrix is very low (see Eq. 3). For the Loamy soil at the initial dried state (h = -3.5 m), the water exchange rate can be more than $4.10^{-5}$ $m^3.m^{-3}.s^{-1}$ and is mainly located in the lower part of the soil column. Because of this initial dried state, the water retention capacity of the soil matrix and the horizontal gradient of the soil matric potential are higher and increase the exchange rate.

For the Silty soil, there are few differences in quantity between the two initial situations, probably because the so-called field capacity is not reached for this column. But there is a difference in the temporality of the exchange rate: the maximum exchange is reached at 1000 s at field capacity and decreases before the end of the rainfall, while in the initial dried state, the exchange rate reaches a maximum at 5600 s and then decreases corresponding to the end of the rainfall over 200 s..

*4.4 Classical vs. advanced version of the model*

The classical version provides better simulations compared to the observed data: this result was expected as the number of parameters to fit is greater for the classical model version (5 parameters to fit) than for the advanced version (3 parameters to fit). Performances of advanced model are nevertheless comparable to the ones obtained by the classical model except for the loamy soil at the initial matric potential of -3.5 m.

To synthetize our results, the different components of the water balance of the soil columns during the experiments are plotted in Figure 9, showing that whatever the soil, the initial water content and model version, we can check that no internal dysfunction or numerical error affects the simulations as the total mass balance is always equal to zero (grey dotted line). Water infiltrates and percolates through the soil mainly through the macropore network, with just a small quantity of the infiltration water remaining stored in the soil.

However, the exchange curves differ according to the version of the model used. The classical one induces little or no exchange for the two initial situations and soils. The advanced one induces little exchange at field capacity: 2 mm for the Silty soil and 0.5 mm for the Loamy soil, but more exchange in the initial dried state: 5 mm for the Silty soil and 10 mm for the Loamy soil. We demonstrate here a different behavior between the two model versions: the classical one generates little water exchange whatever the initial soil conditions, whereas the advanced one generates a larger water exchange that is a function of the initial water content. This highlights the importance of the exchange term and its parameterization for this type of flow model with interacting porosity domains. The number of degrees of freedom is in fact also an issue. Indeed, a large number of parameters will favor the smoothing of experimental results by the model and even if the mass balances are good, the flux distributions do not seem very coherent with the experimental situations, particularly those obtained with the classical version of the model.

## Conclusion

A water flow model accounting for preferential flow made by coupling the Richards' equation to the Kinematic Dispersive Wave (KDW) model with a sink-source term was tested to simulate water infiltration in soils. 5 physically based parameters related to the coupled model (3 parameters for KWD and 2 parameters for the sink-source term) need to be fitted. We showed that the two parameters of the sink-source term may be calculated from 3D images of the soil structure obtained by X-ray CT scan without much loss in fit quality of the drainage dynamics. This is a major benefit of our study as the number of optimized parameters is therefore reduced from 5 to 3 parameters.

Using 3D images of the soil structure combined with the model provide an improved understanding of water exchanges between the macropore network and the soil matrix. As underlined by our sensitivity analysis, this process is of major importance for predicting the overall drainage dynamic when the soil is drier than field capacity. We also demonstrated that the profile of intermacropore spacing is a likely useful parameter to predict the overall water dynamic in natural soils.

However, the formalism used in the model to account for water exchange from macropores to soil matrix is not perfectly adapted to the information provided by the image. More research is needed to improve this model and the sink–source term between macropores and soil matrix with the help of high-speed functional imagery of water flow in undisturbed soil samples. A short-term perspective of this work will also to characterize and quantify the evolution of structural porosity over time as a function of infiltration, drying and combined cycles. As other undertaken approaches, a second step will be the determination of some dynamic relevant structure parameters that could be included in mass transfer models (Bagnall et al. 2019).

## References


Bagnall, D., C.L.S. Morgan, C.C. Molling, J.L. Heilman, and G.W. Moore. 2019. Testing a water redistribution model in a cracked Vertisol at two scales. Vadose Zone J. 18:180173. doi:10.2136/vzj2018.09.0173.

Beven, K., Germann, P., 2013. Macropores and water flow in soils revisited. Water Resour. Res. 49, 3071–3092. https://doi.org/10.1002/wrcr.20156

Beven, K., Germann, P., 1982. Macropores and water flow in soils. Water Resour. Res. 18, 1311–1325. https://doi.org/10.1029/WR018i005p01311

Chen, C., Wagenet, R.J., 1992. Simulation of water and chemicals in macropore soils Part 1. Representation of the equivalent macropore influence and its effect on soilwater flow. J. Hydrol. 130, 105–126.

Clothier, B.E., Green, S.R., Deurer, M., 2008. Preferential flow and transport in soil: progress and prognosis. Eur. J. Soil Sci. 59, 2–13. https://doi.org/10.1111/j.1365-2389.2007.00991.x

Di Pietro, L., 1998. Strategies for describing preferential flow: the continuum approach and cellular-automaton fluids., in: Physical Nonequilibrium in Soils, Modeling and Application., Ann Arbor Press. pp. 437–453.

Di Pietro, L., Lafolie, F., 1991. Water flow characterization and test of a kinematic-wave model for macropore flow in a highly contrasted and irregular double-porosi medium. J. Soil Sci. 42, 551–563. https://doi.org/10.1111/j.1365-2389.1991.tb00102.x

Di Pietro, L., Ruy, S., Capowiez, Y., 2003. Predicting preferential water flow in soils by traveling-dispersive waves. J. Hydrol. 278, 64–75. https://doi.org/10.1016/S0022-1694(03)00124-0

Dirksen, C., 1998. Soil Physics Measurements [WWW Document]. URL https://www.schweizerbart.de/publications/detail/isbn/9783510653867/Dirksen_Soil_Physics_Measurements_GeoE (accessed 7.5.18).

Gerke, H.H., 2012. Macroscopic Representation of the Interface between Flow Domains in Structured Soil. Vadose Zone J. 11, 0. https://doi.org/10.2136/vzj2011.0125

Gerke, H.H., 2006. Preferential flow descriptions for structured soils. J. Plant Nutr. Soil Sci. 169, 382–400. https://doi.org/10.1002/jpln.200521955

Gerke, H.H., van Genuchten, M.T., 1993. A dual-porosity model for simulating the preferential movement of water and solutes in structured porous media. Water Resour. Res. 29, 305–319. https://doi.org/10.1029/92WR02339

Germann, P., Helbling, A., Vadilonga, T., 2007. Rivulet approach to rates of preferential infiltration. Vadose Zone J. 6, 207–220. https://doi.org/10.2136/vzj2006.0115

Germann, P.F., 1990. Preferential Flow and the Generation of Runoff: 1. Boundary Layer Flow Theory. Water Resour. Res. 26, 3055–3063. https://doi.org/10.1029/WR026i012p03055

Germann, P.F., 1985. Kinematic wave approach to infiltration and drainage into and from soil macropores. Am. Soc. Agric. Eng. 28, 745–749.

Germann, P.F., Di Pietro, L., 1996. When is porous-media flow preferential? A hydromechanical perspective. Geoderma 74, 1–21.

Germann, P.F., Di Pietro, L., Singh, V.P., 1997. Momentum of flow in soils assessed with TDR-moisture readings. Geoderma 80, 153–168. https://doi.org/10.1016/S0016-7061(97)00074-8

Gwo, J.P., Jardine, P.M., Wilson, G.V., Yeh, G.T., 1995. A multiple-pore-region concept to modeling mass transfer in subsurface media. J. Hydrol. 164, 217–237.

Hendrickx, J.M.H., Flury, M., 2001. Uniform and preferential flow mechanisms in the vadose zone., in: Conceptual Models of Flow and Transport in the Fractured Vadose Zone., National Research Council, National Academy Press, Washington, DC. pp. 149–187.

Jarvis, N., 1994. The MACRO Model (version 3.1). Swedish University of Agricultural Sciences, Department of Soil Sciences.

Jarvis, N., Boesten, J., 1998. INCORPORATING MACROPORE FLOW INTO FOCUS PEC MODELS JARVIS N., BOESTEN J. 2, HENDRIKS R. 2, KLEIN M. 3, LARSBO M., ROULIER S.

Jarvis, N., Koestel, J., Larsbo, M., 2016. Understanding Preferential Flow in the Vadose Zone: Recent Advances and Future Prospects. Vadose Zone J. 15, 0. https://doi.org/10.2136/vzj2016.09.0075

Jarvis, N.J., Jansson, P.-E., Dik, P.E., Messing, I., 1991. Modelling water and solute transport in macroporous soil. I. Model description and sensitivity analysis. J. Soil Sci. 42, 59–70. https://doi.org/10.1111/j.1365-2389.1991.tb00091.x

Katuwal, S., Norgaard, T., Moldrup, P., Lamande, M., Wildenschild, D., de Jonge, L.W., 2015. Linking air and water transport in intact soils to macropore characteristics inferred from X-ray computed tomography. Geoderma 237, 9–20. https://doi.org/10.1016/j.geoderma.2014.08.006

Mossadeghi-Björklund, M., Arvidsson, J., Keller, T., Koestel, J., Lamandé, M., Larsbo, M., Jarvis, N., 2016. Effects of subsoil compaction on hydraulic properties and preferential flow in a Swedish clay soil. Soil Tillage Res. 156, 91–98. https://doi.org/10.1016/j.still.2015.09.013

Nimmo, J.R., 2012. Preferential flow occurs in unsaturated conditions. Hydrol. Process. 26, 786–789. https://doi.org/10.1002/hyp.8380

Ruy, S., Di Pietro, L., Cabidoche, Y.M., 1999. Numerical modelling of water infiltration into the three components of porosity of a vertisol from Guadeloupe. J. Hydrol. 221, 1–19.

Saltelli, A., Tarantola, S., Chan, K.P.-S., 1999. A Quantitative Model-Independent Method for Global Sensitivity Analysis of Model Output. Technometrics 41, 39–56. https://doi.org/10.2307/1270993

Sammartino, S., Lissy, A.-S., Bogner, C., Van den Bogaert, R., Capowiez, Y., Ruy, S., Cornu, S., 2015. Identifying the Functional Macropore Network Related to Preferential Flow in Structured Soils. Vadose Zone J. 14. https://doi.org/10.2136/vzj2015.05.0070

Sammartino, S., Michel, E., Capowiez, Y., 2012. A Novel Method to Visualize and Characterize Preferential Flow in Undisturbed Soil Cores by Using Multislice Helical CT. Vadose Zone J. 11, 0. https://doi.org/10.2136/vzj2011.0100

Schaap, M.G., Leij, F.J., 2000. Improved Prediction of Unsaturated Hydraulic Conductivity with the Mualem-van Genuchten Model. Soil Sci. Soc. Am. J. 64, 843. https://doi.org/10.2136/sssaj2000.643843x

Schneider, C.A., Rasband, W.S., Eliceiri, K.W., 2012. NIH Image to ImageJ: 25 years of image analysis. Nat. Methods 9, 671–675. https://doi.org/10.1038/nmeth.2089

Tamari, S., Gaudu, J.C., Simonneau, T., 1993. Tensiometric measurement and metastable state of water under tension. Soil Sci. 156, 149–155.

Van Genuchten, M.T., 1980. A closed-form equation for predicting the hydraulic conductivity of unsaturated soils. Soil Sci. Soc. Am. J. 44, 892–898.

Vrugt, J.A., 2016. Markov chain Monte Carlo simulation using the DREAM software package: Theory, concepts, and MATLAB implementation. Environ. Model. Softw. 75, 273–316. https://doi.org/10.1016/j.envsoft.2015.08.013

Vrugt, J.A., Diks, C.G.H., Clark, M.P., 2008. Ensemble Bayesian model averaging using Markov Chain Monte Carlo sampling. Environ. Fluid Mech. 8, 579–595. https://doi.org/10.1007/s10652-008-9106-3

Wind, G.P., 1969. Capillary conductivity data estimated by a simple method.

**Figure legends**

**Fig. 1.** Scheme of the experimental device for lab infiltration experiments composed of a rainfall simulator connected to a pulse pump (not shown in the scheme) and three precision scales (B1, B2 and B3) connected to a computer. The volume recorded by the medical scanner is surrounded by a dotted line.

**Fig. 2.** Flowchart illustrating the main processing steps applied to the 3D images.

**Fig. 3.** Temporal evolutions of the main (dotted lines) and the total (continuous line) contribution indexes of KDW and sink-source term parameters for the classical version of the model. The sensitivity analysis is made with 1200 cumulative drainage curves. The initial water content is given as follow: "FC" for field capacity and "DS" for the dried state (matric potential of -3.5 m).

**Fig. 4.** (a) Drainage curves for the four experiments simulated by the classical and advanced versions of the model (referenced respectively as version 1 and version 2) compared to the experimental data (referenced as observed data). (b) Absolute value of the difference between the experiment and model versions. The initial water content is given by: "FC" for field capacity and "DS" for the dried state (matric potential of –3.5 m).

**Fig. 5.** (a) Storage curves for the four experiments simulated by the classical and advanced versions of the model compared to the experimental data. (b) Absolute value of the difference between the experiment and model versions. The initial water content is given by: "FC" for field capacity and "DS" for dried state (matric potential of – 3.5 m).

**Fig. 6.** Three-dimensional rendering of sample macroporosities at field capacity. The percolating macroporosity is in red and its complementary is in blue. a) Loamy sample. b) Silty sample.

**Fig. 7.** Z-profiles of macroporosities and mean inter-macropore distances. a) Loamy soil. b) Silty soil. The initial water content is referred as "FC" for field capacity and "DS" for dried state (matric potential of – 3.5 m). "P" refers to the percolant part of the macroporosity.

**Fig. 8.** Z-Profiles of water exchange between macropores to soil matrix for the two soil types and the two initial conditions. The initial water content is referred as "FC" for field capacity and "DS" for dried state (matric potential of -3.5 m).

**Fig. 9.** Water mass balance in macropores for the four simulated rainfall experiments with the classical (left) and advanced (right) versions of the model. Cumulated rainfall input (black line), mass balance between water infiltration, drainage and storage (dotted line in grey). Detailed mass balances: surface water infiltration in macropores (blue), water exchanges between macropores to micropores (yellow), drainage (green) and storage in macropores. The initial water content is referred as "FC" for field capacity and "DS" for the dried state (matric potential of –3.5 m).

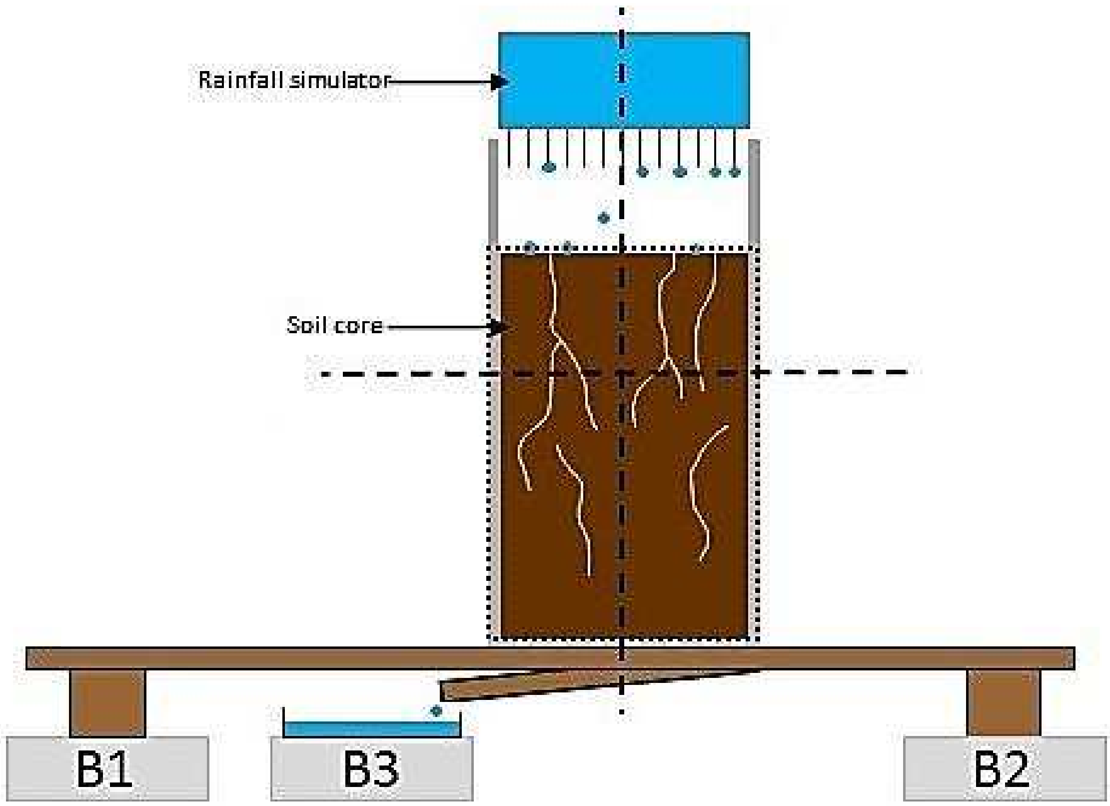
Rainfall simulator
Soil core
B1
B3
B2

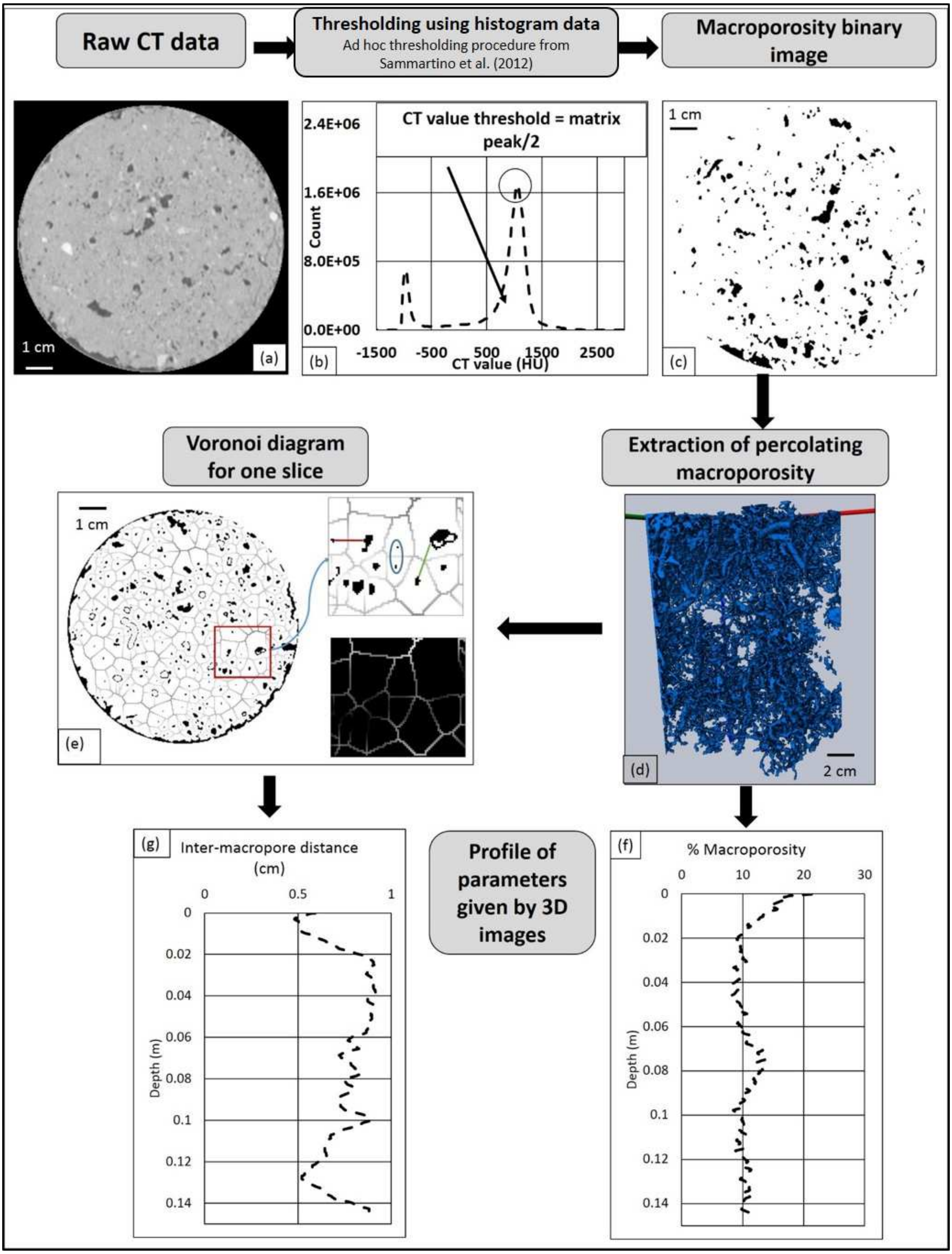

Raw CT data
Thresholding using histogram data
Ad hoc thresholding procedure from Sammartino et al. (2012)
Macroporosity binary image
1 cm
(a)
CT value threshold = matrix peak/2
2.4E+06
1.6E+06
8.0E+05
0.0E+00
Count
-1500
-500
500
1500
2500
CT value (HU)
(b)
1 cm
(c)
Extraction of percolating macroporosity
Voronoi diagram for one slice
1 cm
(e)
(d)
2 cm
(g)
Inter-macropore distance (cm)
0
0.5
1
0
0.02
0.04
0.06
0.08
0.1
0.12
0.14
Depth (m)
Profile of parameters given by 3D images
(f)
% Macroporosity
0
10
20
30
0
0.02
0.04
0.06
0.08
0.1
0.12
0.14
Depth (m)

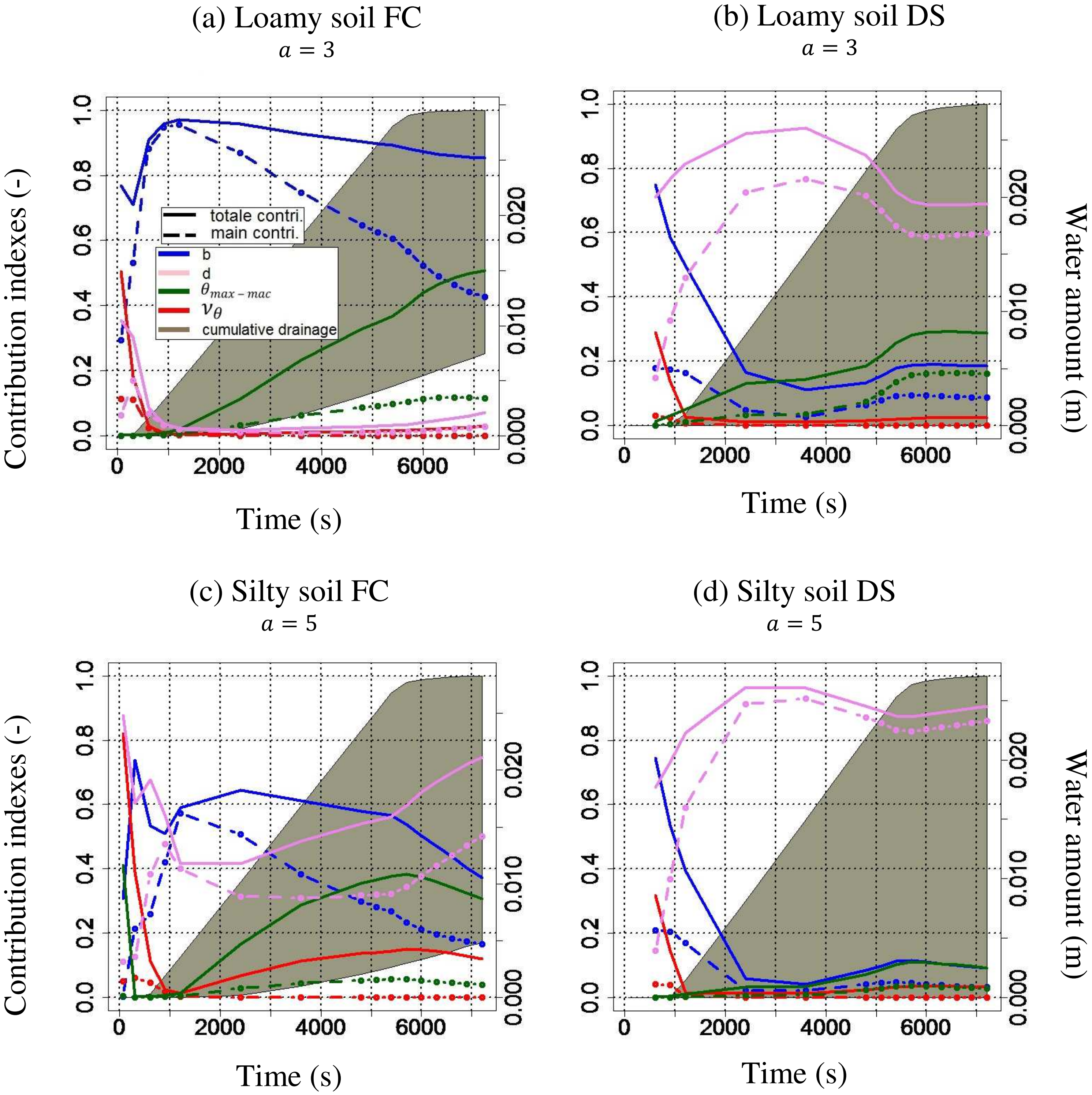

(a) Loamy soil FC
$a = 3$
(b) Loamy soil DS
$a = 3$
(c) Silty soil FC
$a = 5$
(d) Silty soil DS
$a = 5$
Contribution indexes (-)
Water amount (m)
Time (s)
totale contri.
main contri.
b
d
$\theta_{max-mac}$
$\nu_\theta$
cumulative drainage

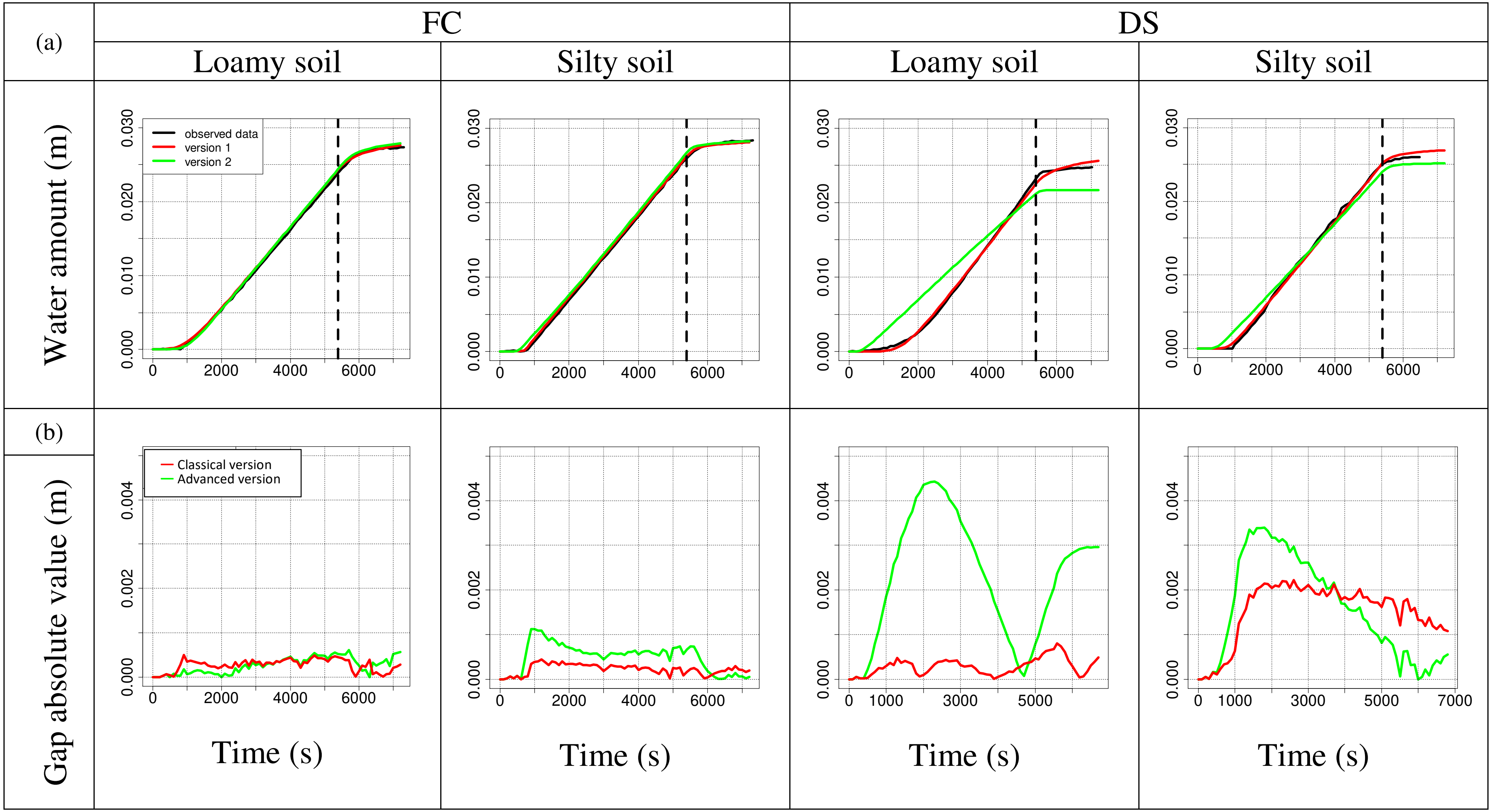

(a)
FC
DS
Loamy soil
Silty soil
Loamy soil
Silty soil
Water amount (m)
observed data
version 1
version 2
(b)
Gap absolute value (m)
Classical version
Advanced version
Time (s)

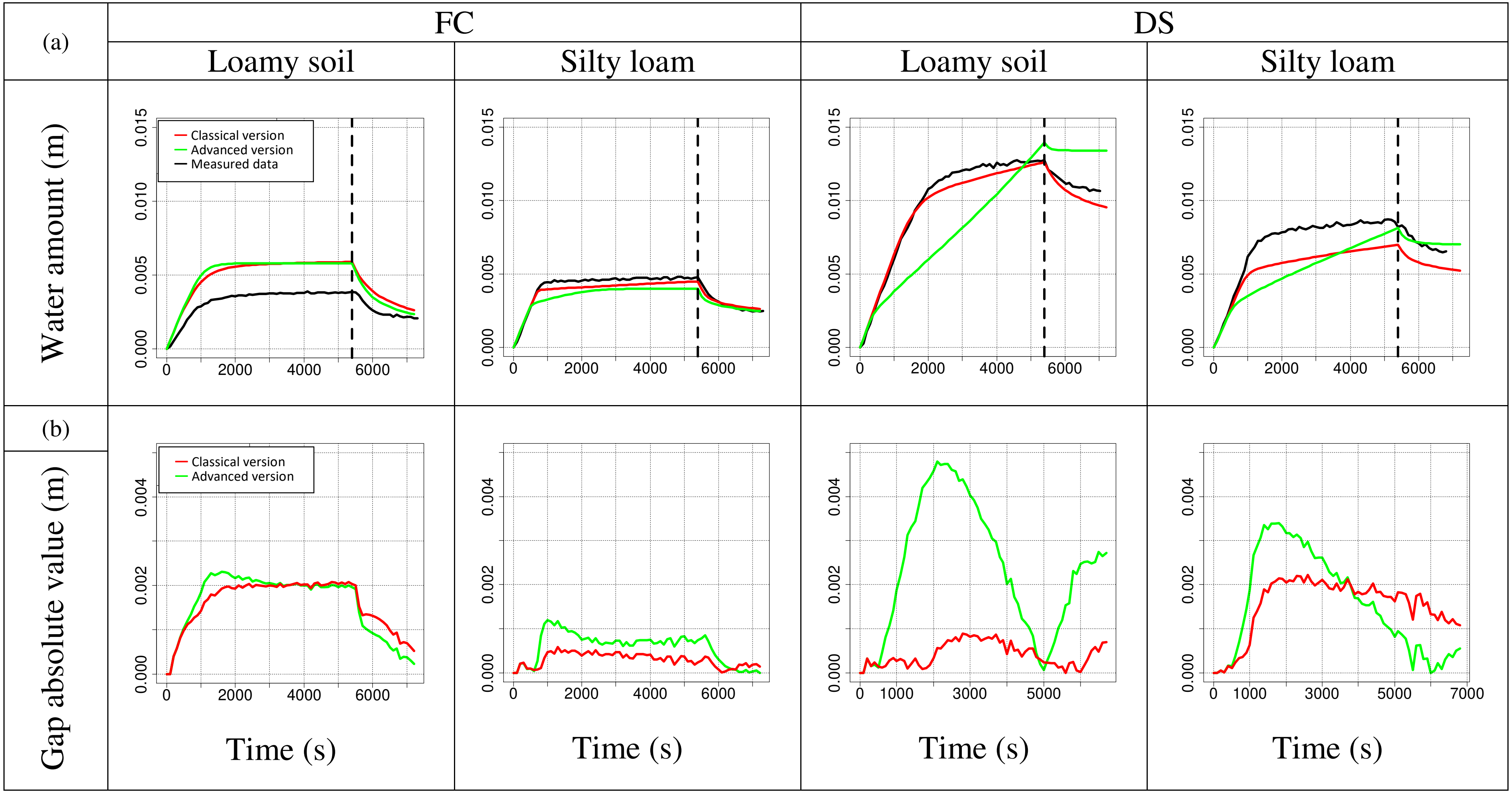
(a)
FC
DS
Loamy soil
Silty loam
Loamy soil
Silty loam
Water amount (m)
Classical version
Advanced version
Measured data
(b)
Gap absolute value (m)
Classical version
Advanced version
Time (s)
Time (s)
Time (s)
Time (s)

a)

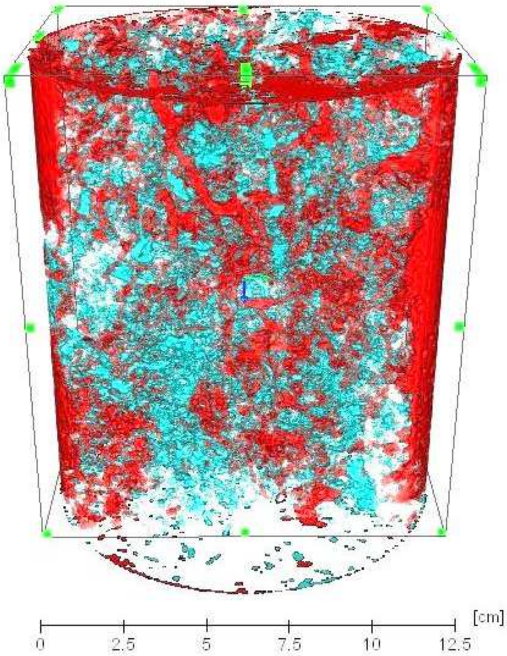


b)

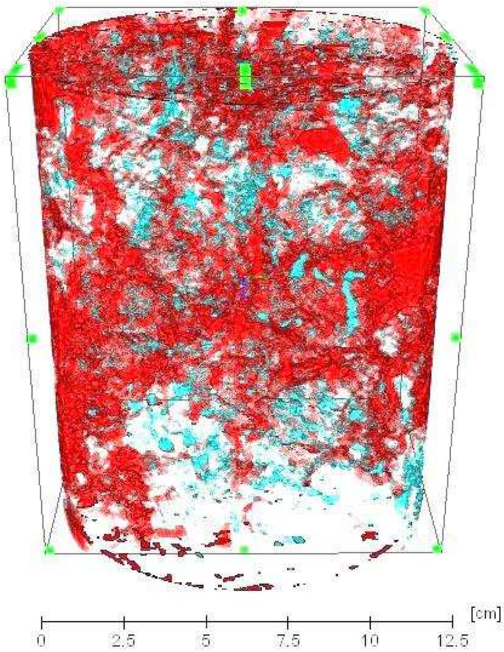

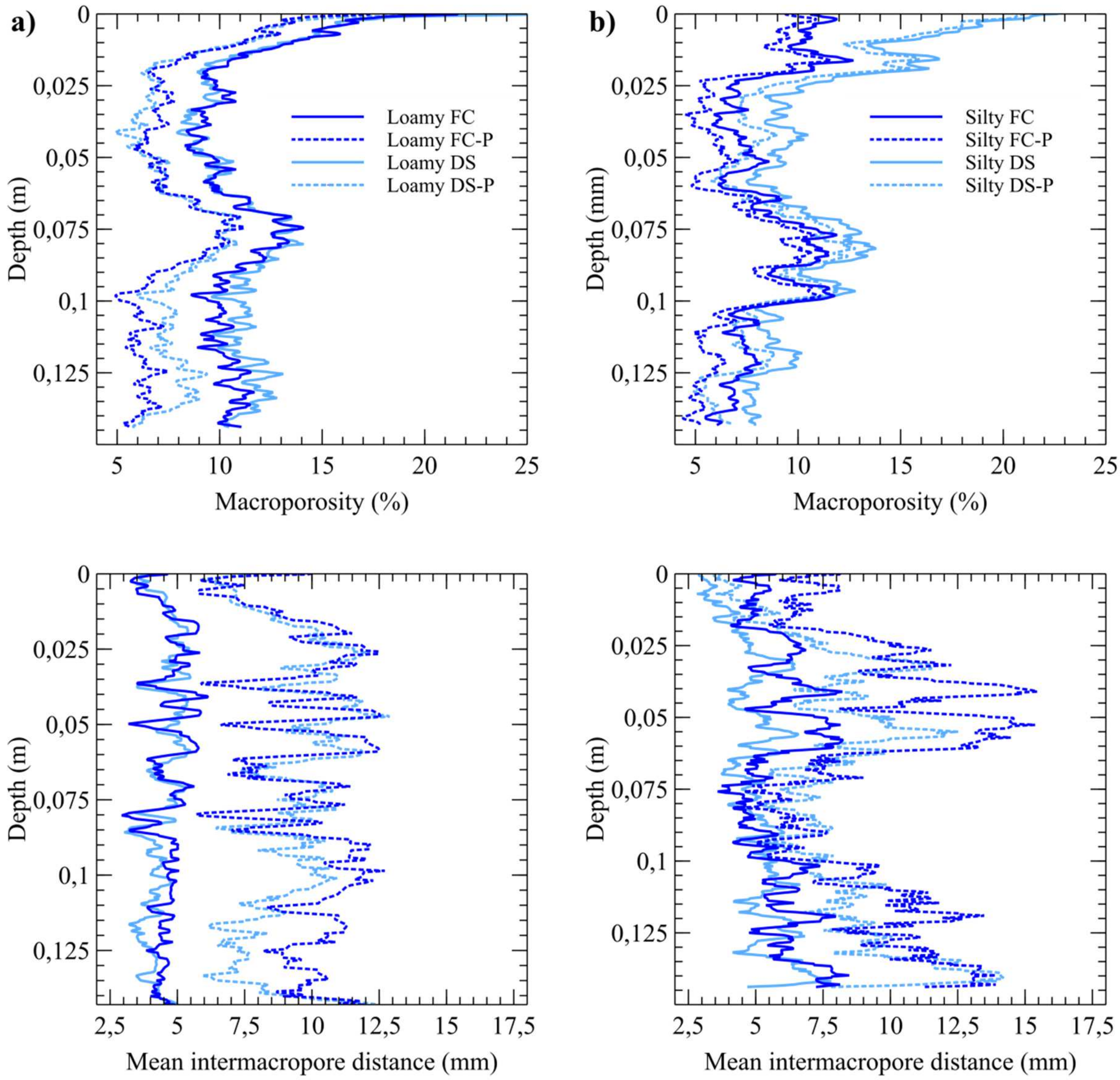
a)
b)
Loamy FC
Loamy FC-P
Loamy DS
Loamy DS-P
Silty FC
Silty FC-P
Silty DS
Silty DS-P
Depth (m)
Depth (mm)
Macroporosity (%)
Mean intermacropore distance (mm)
0
0,025
0,05
0,075
0,1
0,125
5
10
15
20
25
2,5
7,5
12,5
17,5

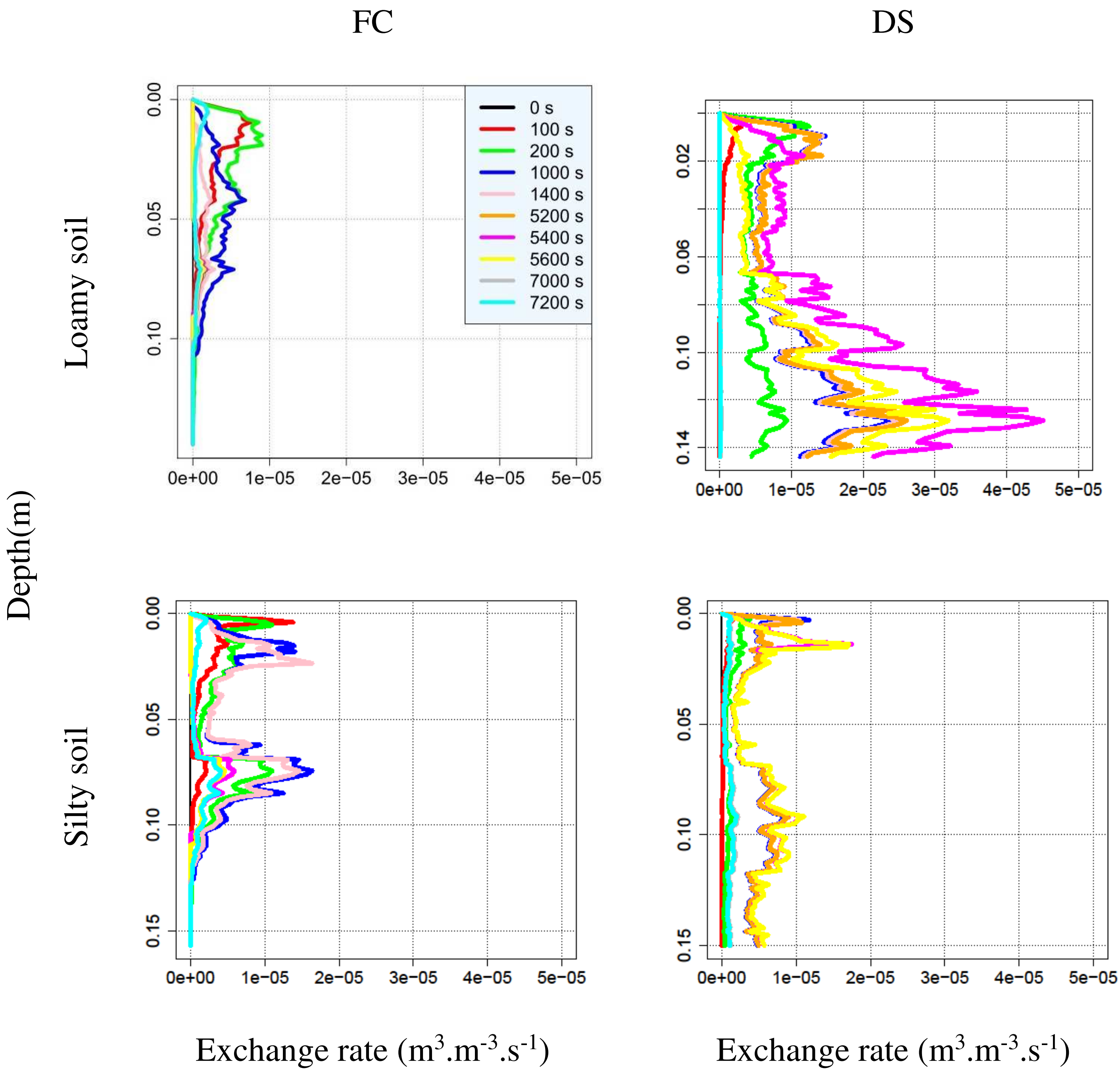
FC
DS
Loamy soil
Silty soil
Depth(m)
0 s
100 s
200 s
1000 s
1400 s
5200 s
5400 s
5600 s
7000 s
7200 s
0e+00
1e−05
2e−05
3e−05
4e−05
5e−05
0.00
0.05
0.10
0.15
0.02
0.06
0.14
Exchange rate (m3.m-3.s-1)
Exchange rate (m3.m-3.s-1)

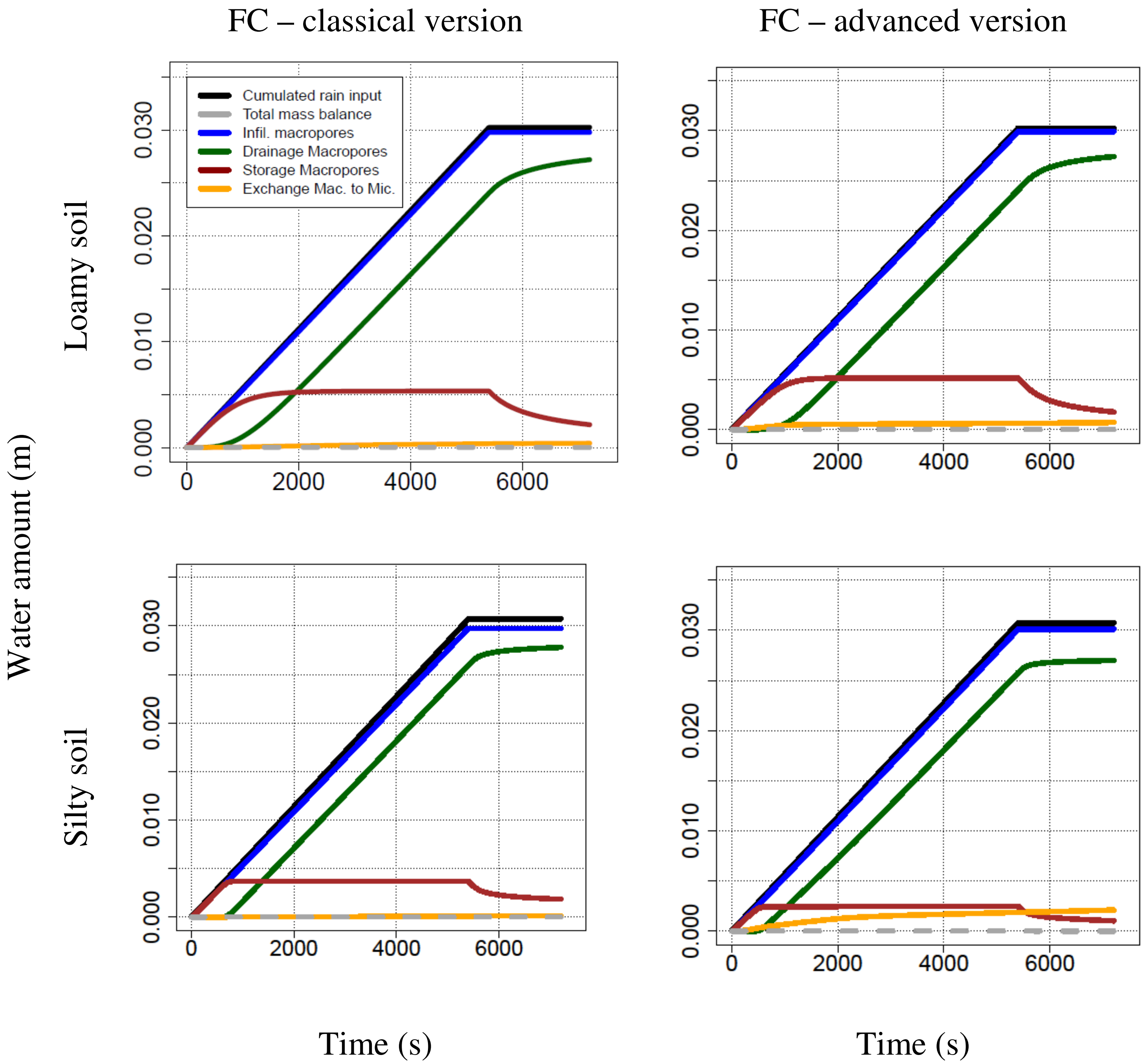

FC – classical version
FC – advanced version
Loamy soil
Silty soil
Water amount (m)
Cumulated rain input
Total mass balance
Infil. macropores
Drainage Macropores
Storage Macropores
Exchange Mac. to Mic.
0.000
0.010
0.020
0.030
0
2000
4000
6000
Time (s)
Time (s)

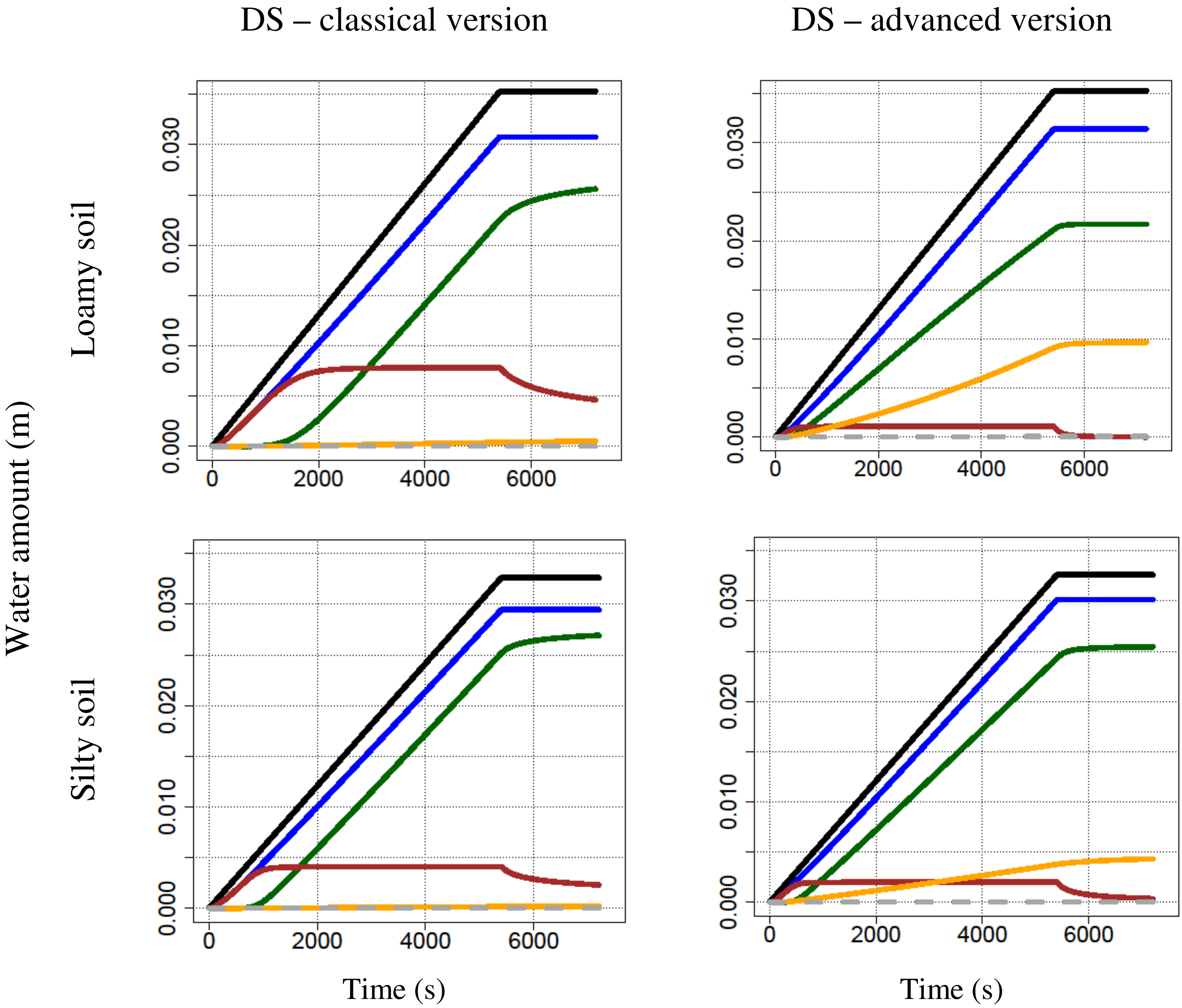

DS – classical version
DS – advanced version
Water amount (m)
Loamy soil
Silty soil
0.000
0.010
0.020
0.030
0
2000
4000
6000
Time (s)

**Table 1.** Soil textural characteristics and sample dimensions.

| Soil core dimensions / Soil texture | Loamy sample | Silty sample |
|---|---|---|
| **Core height (m)** | 0.138 | 0.157 |
| **Core diameter (m)** | 0.125 | 0.125 |
| **Sand fraction (%)** | 37.7 | 1.50 |
| **Silt fraction (%)** | 48.7 | 53.9 |
| **Clay fraction (%)** | 13.6 | 44.6 |

**Table 2.** Parameters of hydrodynamic curves for soils (* fixed values, ** adjusted).

<table>
<tr><th colspan="3">Parameters</th><th>Significance – unity</th><th>Silty soil (0-7 cm) Wind 1</th><th>Silty soil (7-14 cm) Wind 2</th><th>Loamy soil (0-7 cm) Wind 1</th><th>Loamy soil (7-14 cm) Wind 2</th></tr>
<tr><td rowspan="9">Adjusted hydraulic parameters (microporosity domain)</td><td rowspan="4">$\boldsymbol{h(\theta)}$ **</td><td>$\theta_{sat}$</td><td>Saturated water content ($m^3.m^{-3}$)</td><td>0.47</td><td>0.42</td><td>0.37</td><td>0.38</td></tr>
<tr><td>$\theta_{res}$</td><td>Residual water content ($m^3.m^{-3}$) *</td><td>0</td><td>0</td><td>0</td><td>0</td></tr>
<tr><td>$\alpha$</td><td>Structural parameter ($m^{-1}$)</td><td>4.5438</td><td>4.4734</td><td>4.2898</td><td>2.0155</td></tr>
<tr><td>$n$</td><td>Dimensionless parameter (-)</td><td>1.0987</td><td>1.0778</td><td>1.1776</td><td>1.2562</td></tr>
<tr><td rowspan="5">$\boldsymbol{K(\theta)}$ **</td><td>$\theta_{sat}$</td><td>Saturated water content ($m^3.m^{-3}$)</td><td>0.46</td><td>0.42</td><td>0.43</td><td>0.47</td></tr>
<tr><td>$\theta_{res}$</td><td>Residual water content ($m^3.m^{-3}$)</td><td>0</td><td>0</td><td>0</td><td>0</td></tr>
<tr><td>$K_{sat-mic}$</td><td>Saturated fitted hydraulic conductivity ($m.s^{-1}$)</td><td>$4.55.10^{-08}$</td><td>$1.82.10^{-7}$</td><td>$6.71.10^{-07}$</td><td>$2.50.10^{-06}$</td></tr>
<tr><td>$n$</td><td>Dimensionless parameter (-)</td><td>1.2755</td><td>1.1815</td><td>1.4285</td><td>1.4268</td></tr>
<tr><td>$tortuosity$</td><td>Tortuosity factor (-) *</td><td>0.5</td><td>0.5</td><td>0.5</td><td>0.5</td></tr>
<tr><td rowspan="4">Measured hydraulic parameters on Wind samples (undisturbed samples: microporosity and macroporosity domains)</td><td colspan="3">$\boldsymbol{\theta_{init-meas}}$ measured at the beginning of the experiment ($m^3$ $m^{-3}$)</td><td>0.45</td><td>0.42</td><td>0.37</td><td>0.38</td></tr>
<tr><td colspan="3">Porosity ($m^3$ $m^{-3}$)</td><td>0.45</td><td>0.43</td><td>0.48</td><td>0.47</td></tr>
<tr><td colspan="3">$K_{sat-meas}$ ($m.s^{-1}$)</td><td>$3.16.10^{-04}$</td><td>$6.58.10^{-04}$</td><td>$3.38.10^{-04}$</td><td>$3.54.10^{-05}$</td></tr>
<tr><td colspan="3">Bulk density ($g.cm^{-3}$)</td><td>1.48</td><td>1.52</td><td>1.40</td><td>1.41</td></tr>
</table>

**Table 3.** KDW and sink – source term parameters, and range of variation for the DREAM algorithm.

| Range of values | Macropores shape parameter | Kinematic coefficient | Diffusion coefficient | Inter – macropore distance | Maximal water content in macroporosity |
|---|---|---|---|---|---|
| | $a\ (-)$ | $b\ (m.s^{-1})$ | $\nu_\theta\ (m)$ | $d\ (m)$ | $\theta_{max-mac}(m^3.m^{-3})$ |
| **Classical version** | $[\,1\,;\ 6]$ | $[\frac{b_{th}}{5}; b_{th} \times 5]$ | $[\,5.10^{-3}; 10^{-1}]$ | $[10^{-4}; 10^{-1}]$ | $\left[\frac{\theta_{max-mac-meas}}{2}; \theta_{max-mac-meas} \times 2\right]$ |
| **Advanced version** | $[\,1\,;\ 6]$ | $[\frac{b_{th}}{5}; b_{th} \times 5]$ | $[\,5.10^{-3}; 10^{-1}]$ | Calculated from CT profile | Calculated from CT profile |

**Table 4.** Parameters of KDW and of the sink-source term, estimated for the classical and advanced versions of the model. "FC" refers to the field capacity state and "DS" refers to the dried state at h = -3.5 m. * Values calculated from CT images.

| Parameters | FC | | | | DS | | | |
|---|---|---|---|---|---|---|---|---|
| | Loamy soil | | Silty soil | | Loamy soil | | Silty soil | |
| | Classical | Advanced | Classical | Advanced | Classical | Advanced | Classical | Advanced |
| $\boldsymbol{a}\ (-)$ | 2.5 | 2.5 | 5.0 | 5.3 | 4.4 | 1.7 | 5.4 | 2.8 |
| $\boldsymbol{b}\ (\mathbf{m.s^{-1}})$ | $2.3.10^{-2}$ | $2.3.10^{-2}$ | $9.1.10^{+2}$ | $2.1.10^{+4}$ | 2.2 | $3.2.10^{-2}$ | $1.7.10^{+3}$ | 1.3 |
| $\boldsymbol{\nu_\theta}\ (\boldsymbol{m})$ | $1.1.10^{-4}$ | $1.1.10^{-5}$ | $1.1.10^{-5}$ | $1.1.10^{-5}$ | $1.2.10^{-3}$ | $2.8.10^{-5}$ | $8.7.10^{-4}$ | $3.8.10^{-5}$ |
| $\boldsymbol{d}\ (\boldsymbol{m})$ | 0.027 | 0.0083 | 0.095 | 0.0087 | 0.066 | 0.0074 | 0.044 | 0.0075 |
| $\boldsymbol{\theta_{max-mac}}\ (-)$ | 0.058 | 0.056* | 0.074 | 0.054* | 0.072 | 0.060* | 0.066 | 0.067* |

**Table 5.** Entire and percolating macroporosity, mean inter-macropore distance for the two initial water contents and the two studied soils, and the percolating fraction of the entire macroporosity. "FC" refers to the field capacity state and "DS" refers to the dried state at h = -3.5 m.

| **Macroporosity type** | **Entire** | | | | **Percolating** | | | |
|---|---|---|---|---|---|---|---|---|
| **Soil type & initial water content** | Loamy FC | Loamy DS | Silty FC | Silty DS | Loamy FC | Loamy DS | Silty FC | Silty DS |
| **Macroporosity (%)** | 10.9 | 11.2 | 8.4 | 10.7 | 7.7 | 8.2 | 7.2 | 9.3 |
| **Mean inter–macropore distance (mm)** | 4.6 | 4.4 | 5.8 | 5.0 | 9.8 | 9.2 | 9.3 | 7.8 |
| **Fraction of percolating macroporosity (%)** | 70.6 | 72.6 | 85.5 | 87.4 | 100 | | | |